Geochimica et Cosmochimica Acta xxx (xxxx) xxx

Contents lists available at ScienceDirect

Geochimica et Cosmochimica Acta

journal homepage: www.elsevier.com/locate/gca

The I/Ca paleo-oxygenation proxy in planktonic foraminifera: A multispecies core-top calibration

Anya V. Hess [a,b,*], Yair Rosenthal [a,c], Xiaoli Zhou [d], Kaixuan Bu [c]

[a] Earth and Planetary Sciences, Rutgers, the State University of New Jersey, New Brunswick, NJ, USA
[b] Geology and Geophysics, Woods Hole Oceanographic Institution, Woods Hole, MA, USA
[c] Marine and Coastal Sciences, Rutgers, the State University of New Jersey, New Brunswick, NJ, USA
[d] State Key Laboratory of Marine Geology, Tongji University, Shanghai, China

ARTICLE INFO

Associate editor: Thomas M. Marchitto

Keywords:
Planktonic foraminifera
I/Ca
Ocean oxygenation
Oxygen deficient zone

ABSTRACT

Iodine-to-calcium ratios (I/Ca) in planktonic foraminifera have been used for the reconstruction of upper ocean oxygenation in the geologic past, particularly for detecting oxygen-deficient zones (ODZs). We examine the response of I/Ca in various planktonic foraminifera species from core-top sediment samples to changes in iodate and the minimum oxygen concentration in the uppermost 500 m of the water column ($[O_2]_{min}$). Published data are concentrated in the Atlantic Ocean and in areas with either very high or very low oxygen concentrations. Our study supplements those studies using samples from the GEOTRACES GP16 transect through the southern lobe of the eastern tropical Pacific oxygen deficient zone and areas in the western equatorial Pacific and Atlantic Ocean characterized by intermediate oxygen concentrations ($[O_2]_{min}$ of 100–170 μmol/kg). We use Mg/Ca values measured alongside I/Ca to determine apparent calcification depth for foraminifera in the tropical Pacific. We find that I/Ca values in foraminifera species from different water depth habitats vary predictably based on patterns in iodate concentration spatially and with depth in the upper water column. In well-oxygenated areas of the ocean, I/Ca values are relatively high, with the highest values in deep subsurface foraminifera species that lived furthest from the mixed layer where primary productivity converts iodate to iodide and organic iodine. In ODZs, I/Ca values are relatively low and this pattern reverses, with the lowest I/Ca values in deep subsurface species living near or within the ODZ where iodate is used as an electron acceptor during oxidation of sinking organic matter. The difference between deep subsurface and surface I/Ca values can therefore provide another line of evidence for identifying the core of an ODZ in paleoceanographic records. This study suggests that the large scatter in the I/Ca data reflects the complexity of the relationship between the distribution of iodate and dissolved oxygen through the water column and spatially, and the depths at which foraminifera calcify with respect to that distribution. We employ a linear correlation between I/Ca and $[O_2]_{min}$ as the most parsimonious explanation for this complex system. Across the eastern tropical Pacific transect, I/Ca responds to small oxygenation changes on the order of 10s of μmol/kg, suggesting that I/Ca may be able to detect small relative changes in oxygenation of this magnitude in consecutive downcore samples. We note, however, that interpretation of such changes is strengthened by the use of additional paleo-oxygenation proxies.

1. Introduction

Over the past half century, shallow waters of the oceans (<700 m water depth) have been losing oxygen in response to rising temperatures (Stramma and Schmidtko, 2021), with dire consequences for marine ecosystems and the humans who depend upon them. To understand this trend and predict its response to continued climate change, we turn to the past, reconstructing how ocean oxygenation has responded to climate change in the geologic past. Studies have shown that during some past warm climates, oxygen concentration in currently oxygen-depleted regions may have increased, in contrast to recent deoxygenation trends (e.g., Auderset et al., 2022; Hess et al., 2023). For this type of work, proxies capable of reconstructing oxygen concentrations in the upper water column are needed. The iodine-to-calcium ratio (I/Ca) in foraminifera is one such proxy (e.g., Lu et al., 2010, 2016; Hoogakker et al., 2018; Hess et al., 2023).

* Corresponding author at: Earth and Planetary Sciences, Rutgers, the State University of New Jersey, New Brunswick, NJ, USA.
E-mail address: anya.hess@gmail.com (A.V. Hess).

https://doi.org/10.1016/j.gca.2025.01.018
Received 8 May 2024; Accepted 16 January 2025
Available online 22 January 2025

Iodine in the ocean exists primarily as the thermodynamically favorable oxidized form iodate (IO_3^-), with select areas also containing significant portions of the reduced form iodide (I^-) (Wong, 1991). Iodate is converted to iodide by redox process in very low oxygen areas such as in shallow-water (10s to 100s of meters) oxygen-deficient zones (ODZs) and by primary production in the euphotic zone (Wong, 1991; Hepach et al., 2020). In the open ocean, iodate concentrations are relatively high at the surface (>~250 nmol/L) and higher in the subsurface. In ODZs, iodate concentrations are relatively low at the surface (<~250 nmol/L) and near zero in the subsurface, with surface values depleted due to the combined effects of increased primary productivity and mixing with low-iodate waters from the underlying ODZ water mass (Lu et al., 2016). The relatively slow (months to years) oxidation of iodide to iodate allows low iodate concentrations to persist in surface waters despite their high oxygen concentrations (Chance et al., 2014). The signal of low iodate concentrations above ODZs is preserved in foraminifera as low I/Ca ratios because iodate is incorporated into their carbonate tests, possibly substituting for the carbonate ion, whereas iodide is not (Lu et al., 2010). Recent studies have illustrated the promise of this proxy to reconstruct upper ocean oxygenation during the geologic past, including

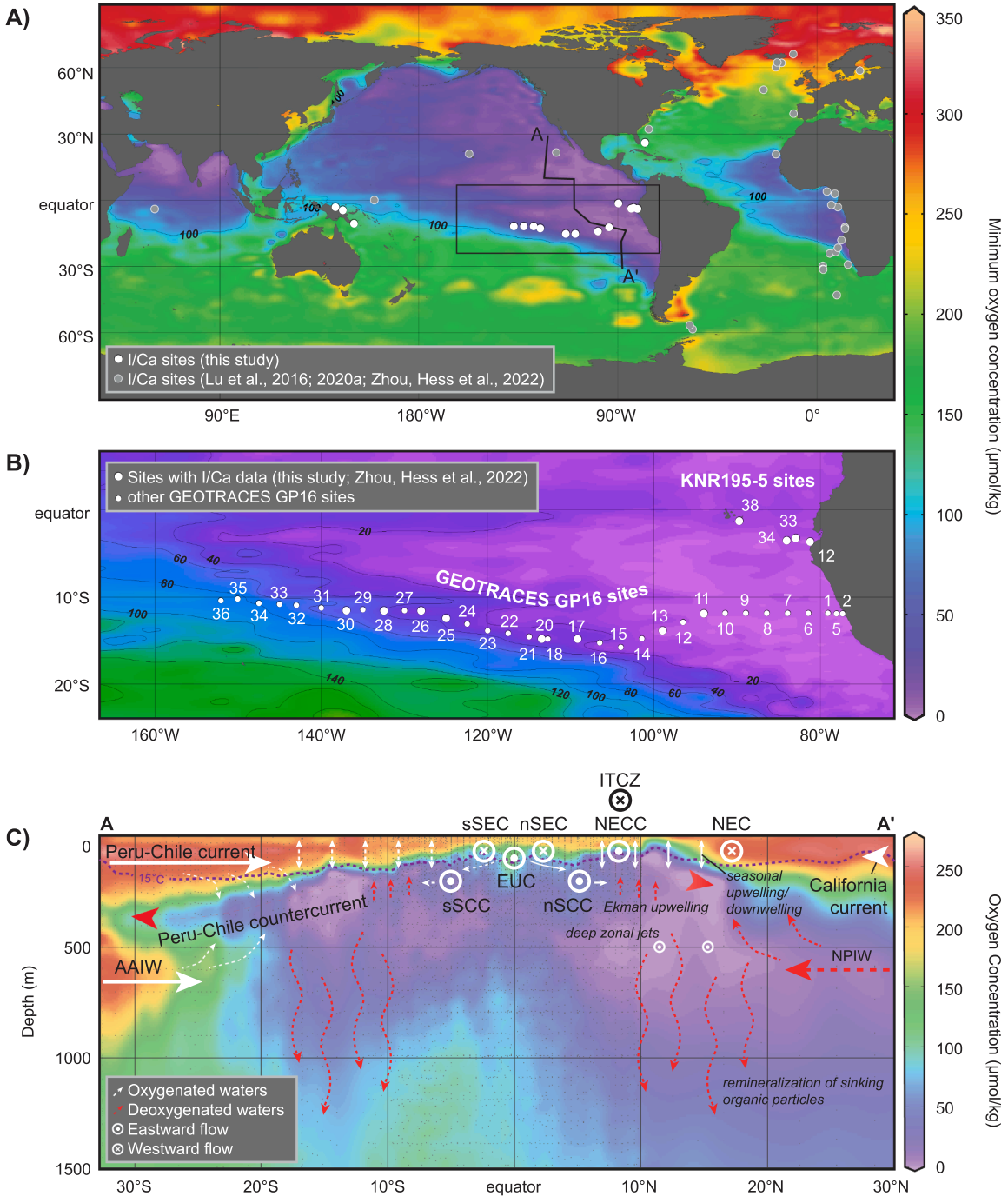

Fig. 1. Oxygenation maps and cross section. (A) Map of minimum oxygen concentration in the water column with I/Ca sites. Area of black box is shown in part B and cross section A-A' is shown in part C. (B) Southeastern tropical Pacific ODZ sites. See Fig. 2 for water-column properties at GEOTRACES GP16 sites. (C) North-south cross section through the ETP ODZ showing water masses (regular text) and processes (italics) responsible for oxygenation (white) and deoxygenation (red). Note different color scale from other panels. Concepts from Fiedler and Talley (2006), Fuenzalida et al. (2009), Helly and Levin (2004), Kessler (2006), Margolskee et al., (2019), Schott et al. (2004), and references therein. Purple dashed line is 15 °C line above which phytoplankton live (Fiedler and Talley, 2006).

during Quaternary glacial-interglacial cycles (Lu et al., 2016; Hoogakker et al., 2018), the Miocene Climatic Optimum (Hess et al., 2023), and the Paleocene-Eocene thermal maximum (Zhou et al., 2014). I/Ca has also been measured in bulk carbonate material as a proxy for surface-water oxygenation (Hardisty et al., 2014, 2017; Zhou et al., 2015; Lu et al., 2017, 2018) and in benthic foraminifera as a proxy for bottom-water oxygenation (Glock et al., 2014, 2016; Taylor et al., 2017; Lu et al., 2020b, Lu et al., 2021, 2022).

Current calibrations for the I/Ca proxy in planktonic foraminifera are based on a global dataset of surface (core-top) sediments with the majority of sites from hypoxic to oxic areas of the Atlantic Ocean (Lu et al., 2016, 2020a). Compared to the Atlantic, the Pacific has been sparsely sampled for core-top I/Ca data (Lu et al., 2016, 2020a). The eastern tropical Pacific (ETP) contains one of the largest and most oxygen-depleted ODZs in the world (Fig. 1); old, oxygen-depleted, nutrient-enriched waters upwell through Ekman pumping, fueling biological productivity, and the remineralization of sinking organic matter drives down oxygen concentrations below the thermocline (Karstensen et al., 2008). Shallow-water productivity, stronger and shallower to the east, is apparent in increased fluorescence eastward and corresponds with a shallower thermocline and oxycline to the east and a zone of iodate reduction that is likewise shallower and thicker to the east (Fig. 2). The ETP ODZ is divided into a northern and southern lobe (N-ETP ODZ and S-ETP ODZ, respectively) by the oxygenated equatorial undercurrent (Fig. 1C). The N-ETP ODZ is larger because, while both lobes receive ventilated Southern Ocean waters, the N-ETP receives ~30 % of its waters from the unventilated North Pacific (Margolskee et al., 2019). Here, we present new core-top I/Ca data from the east–west GEOTRACES GP16 transect, which traverses the S-ETP ODZ (Fig. 1B), as well as additional data from oxic sites in the western tropical Pacific and Atlantic, including areas at intermediate oxygen concentrations that are thus far under-sampled (Fig. 1A white dots). We also evaluate the role of calcification depth on I/Ca for foraminifera species that occupy different water depths from surface to within and below the thermo- and oxycline.

2. Material and methods

We have measured trace elemental composition in planktonic foraminifera from core-top (<6 cm core depth) sediment samples from globally diverse locations (Fig. 1A, Table 1). We targeted sites with intermediate oxygen concentrations from the western tropical Pacific (RR1313 Cruise) and Atlantic Oceans (VM and OC205-2 Cruises) and a transect from the GEOTRACES GP16 Cruise, which traversed the southern lobe of the poorly oxygenated S-ETP ODZ at ~10°S (Fig. 1A–B). The most westward GP16 site sampled is Site 30 because sites westward of this are at water depths below the calcite compensation depth (CCD, >~4 km) and contain insufficient carbonate material for I/Ca analysis (German, 2017). Sites from the Ecuador margin (KNR195-5 Cruise) in the center of this ODZ are also included. All samples from the Pacific, including the GP16 transect, are from multicorers, known to capture the sediment–water interface. One site from the Atlantic is a box core, also designed to capture the sediment–water interface. In areas with low sedimentation rates like the S-ETP ODZ (Bender et al., 1971), core-top samples can represent thousands of years of deposition. GP16 samples, from the upper 1–4 cm of sediment, likely encompass hundreds to a few thousands of years of deposition based on sedimentation rates of 0.45–1.50 cm/kyr at nearby sites (Bender et al., 1971). We note, however, that core-top foraminifera samples yield I/Ca values similar to those from down-core samples, unlike plankton-tow samples, which can have I/Ca values an order of magnitude lower (Lu et al., 2023; Winkelbauer et al., 2023), so core-top data appear to be more appropriate for calibrating down-core data.

The trace elemental composition of planktonic foraminifera was compared to water-column data at or near each site. For GP16 sites, oxygen and temperature data were taken from GT-C CTD downcasts at each site (Moffett et al., 2020) and iodate and iodide concentrations were taken from accompanying bottle data (Cutter, 2017) collected within ~2 days of the CTD. For non-GP16 sites, we used oxygen and temperature data from World Ocean Database 2018 (Boyer et al., 2018), choosing the nearest site with available data at an appropriate resolution (e.g., resolution <~100 m depth increments).

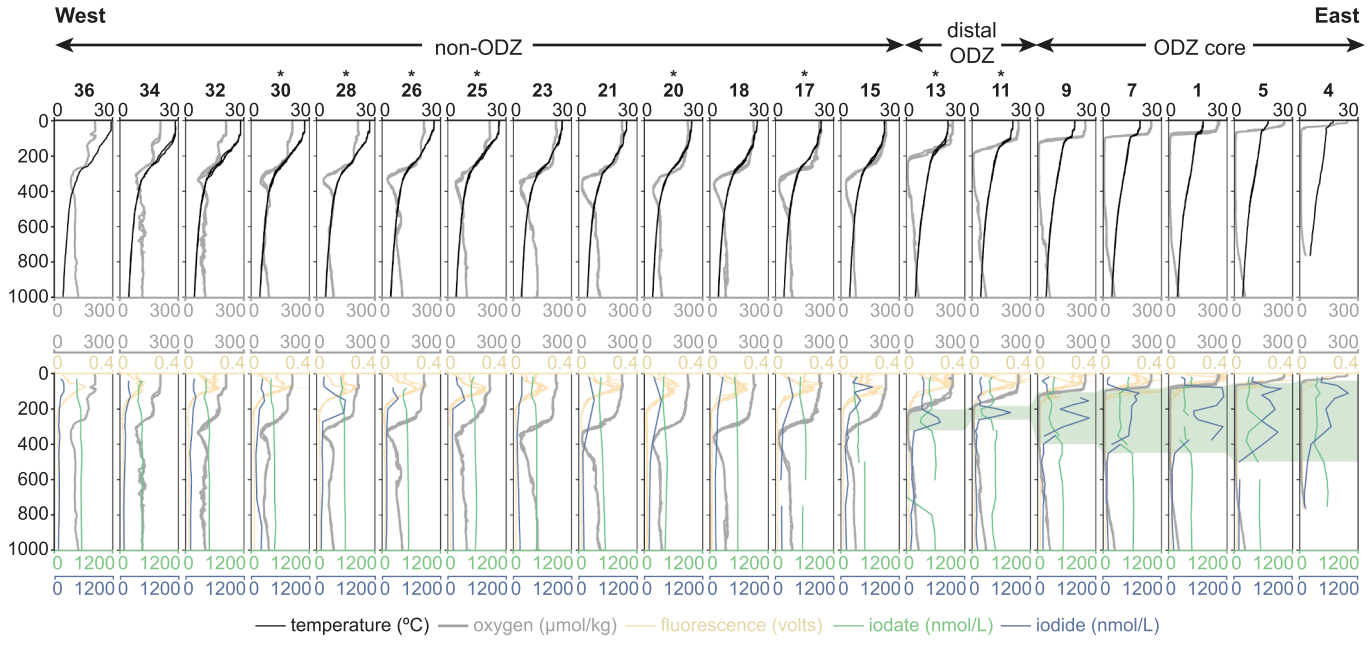

Fig. 2. Water-column profiles for GEOTRACES GP16 sites. Showing relationship between thermocline and oxycline in top row and relationship between iodine speciation, oxygenation, and productivity in bottom row. Sites are labeled across the top; stars indicate sites with I/Ca core top data. Green shading indicates area with decreased iodate and increased iodide concentrations within the ODZ. Data from all casts are shown. ODZ core, distal ODZ, and non-ODZ labels indicate oxygen, iodate, and iodide patterns used in the conceptual model (Fig. 4). Temperature, oxygen concentrations, and fluorescence CTD data from Moffett et al. (2020). Iodine data from Cutter (2017), taken within days of CTD data.

Table 1
Sites with I/Ca data and nearby sites from which water-column oxygen concentrations are taken. * indicates sites with local oxygen variability. MC = multi-core, BC = box core, GGC = gravity core, PC = piston core, KC = kasten core.

Site	Sample sediment depth (cm below seafloor)	Region	Site latitude (decimal degrees)	Site longitude (decimal degrees)	Site water depth (m)	Nearby cast site (wod18)	Nearby cast site latitude (decimal degrees)	Nearby cast site longitude (decimal degrees)	Source for I/Ca data
GP16 MOC11 (MC)	1–2	Pacific	−11.9997	−94	3671	self from GEOTRACES GP16	N/A	N/A	this study
GP16 MOC13 (MC)	1–2	Pacific	−14.0002	−99	3859	self from GEOTRACES GP16	N/A	N/A	this study
GP16 MOC17 (MC)	1–4	Pacific	−14.9998	−109.1905	3718	self from GEOTRACES GP16	N/A	N/A	this study
GP16 MOC20 (MC)	1–2	Pacific	−15.0002	−113.5003	3187	self from GEOTRACES GP16	N/A	N/A	this study
GP16 MOC25 (MC)	1–2	Pacific	−12.5422	−124.9995	3951	self from GEOTRACES GP16	N/A	N/A	this study
GP16 MOC26 (MC)	1–2	Pacific	−11.6702	−128	3994	self from GEOTRACES GP16	N/A	N/A	this study
GP16 MOC28 (MC)	1–2	Pacific	−11.6252	−132.5003	4048	self from GEOTRACES GP16	N/A	N/A	this study
GP16 MOC30 (MC)	1–2	Pacific	−11.5805	−136.981	4113	self from GEOTRACES GP16	N/A	N/A	this study
KNR195-5 MC12-F (Site 6)	2–3	Pacific	−3.7105	−81.1153	378	WOD Peru 22022389 (C)	3.717 S	−81.112	this study
KNR195-5 MC33-F (Site 13)	2–3	Pacific	−3.2237	−82.9142	2949	WOD Ecuador 8419866 (B)	3.17 S	−83	Zhou, Hess et al. (2022)
KNR195-5 MC34-F (Site 14)	2–3	Pacific	−3.5975	−83.9632	3224	WOD Peru 22020282 (B)	3.63 S	−83.926	Zhou, Hess et al. (2022)
KNR195-5 MC38-E (Site 15)	0–1	Pacific	−1.2657	−89.6993	597	WOD Germany 120103785 (B)	1.061 S	−89.425	Zhou, Hess et al. (2022)
RR1313 21MC-E + F (Site 8)	1–2	Pacific	−4.327	145.511	760	WOD United States 854909 (B)	3.842 S	145.323	this study
RR1313 28MC-F + G (Site 11)	1–2	Pacific	−2.927	142.266	1081	WOD Japan 9588456 (C)	2.717 S	142.001	this study
RR1313 2MC-F + D (Site 2)*	1–2	Pacific	−10.412	150.647	545	WOD Australia 10161687 (C)	9.991 S	150.508	this study
MW97-20 MC20D	0–0.5	Pacific	−0.00417	159.8693	2958	WOD Soviet Union 11180668 (B)	0	159.83	Zhou, Hess et al. (2022)
MW97-20 MC9E	0–0.5	Pacific	−0.00417	159.8693	2015	WOD Soviet Union 11180668 (B)	0	159.83	Zhou, Hess et al. (2022)
MW98-13 26GGC	6.5	Pacific	20.84	−157.2	1200	WOD United States 189628 (B)	20.8 N	−157.5	Zhou, Hess et al. (2022)
OC205-2 57BC	0–2	Atlantic	26.16	−77.72	1243	WOD United States 251321 (B)	25.8	−77.18	this study
OC205-2 60BC	0–2	Atlantic	26.14	−77.74	1312	WOD United States 251321 (B)	25.8	−77.18	Zhou, Hess et al. (2022)
V22-154 (PC)	0–2	Atlantic	−31.2	2.8	1618	WOD United States 22006737 (C)	−31.176	2.992	this study, Zhou, Hess et al. (2022), Lu et al. (2020a)
V27-214 (PC)	3–5	Atlantic	−31.1	2.7	1752	WOD United States 21993663 (C)	−31.018	2.643	this study, Zhou, Hess et al. (2022), Lu et al. (2020a)
V29-120 (PC)	4–6	Atlantic	−29.8	2.6	1805	WOD Soviet Union 771070 (B)	−29.93	2.43	this study, Zhou, Hess et al. (2022), Lu et al. (2020a)

(continued on next page)

Table 1 (*continued*)

Site	Sample sediment depth (cm below seafloor)	Region	Site latitude (decimal degrees)	Site longitude (decimal degrees)	Site water depth (m)	Nearby cast site (wod18)	Nearby cast site latitude (decimal degrees)	Nearby cast site longitude (decimal degrees)	Source for I/Ca data
M39059-2 (BC)		Atlantic	39.06667	−10.535	1605	WOD Soviet Union 7757136 (B)	38.95 N	−10.467	Zhou, Hess et al. (2022)
GeoB1720-2 (MC)	core top	Atlantic	−29	14	1997	WOD United States 15560812 (B)	−28.917	13.967	Lu et al. (2020a)
RC13-201 (PC)	core top	Atlantic	3.9	4.5	1856	WOD France 3329638 (B)	4 N	4.267	Lu et al. (2020a)
RC13-202 (PC)	core top	Atlantic	2.8	8.1	1035	WOD France 3327298 (B)	2.717 N	8	Lu et al. (2020a)
RC13-220 (PC)	core top	Atlantic	−12.2	12.6	1760	WOD Portugal 670539 (B)	12.23 S	12.63	Lu et al. (2020a)
RC13-221 (PC)	core top	Atlantic	−12.8	12.6	1995	WOD Unknown 21180634 (C)	12.733 S	12.62	Lu et al. (2020a)
RC17-44 (PC)*	core top	Atlantic	−29.8	15	377	WOD South Africa 8751775 (B)	29.83 S	15	Lu et al. (2020a)
V12-58 (PC)*	core top	Atlantic	–32.2	16.3	459	WOD South Africa 17363467 (C)	32.31 S	16.315	Lu et al. (2020a)
V12-59 (PC)*	core top	Atlantic	–32.2	16.3	424	WOD South Africa 17363467 (C)	32.31 S	16.315	Lu et al. (2020a)
V14-70 (PC)*	core top	Atlantic	−34.6	17.6	1067	WOD South Africa 9927460 (C)	34.612 S	17.651	Lu et al. (2020a)
V16-49 (PC)*	core top	Atlantic	−31.9	16.3	410	WOD South Africa 8751766 (B)	31.927 S	16.273	Lu et al. (2020a)
V19-228 (PC)*	core top	Atlantic	−34.5	17.7	508	WOD South Africa 9927459 (C)	34.493 S	17.804	Lu et al. (2020a)
V19-238 (PC)*	core top	Atlantic	–32.6	16.2	1553	WOD South Africa 17363452 (C)	32.614 S	16.204	Lu et al. (2020a)
V20-202 (PC)*	core top	Atlantic	−30.5	15.4	327	WOD South Africa 17364119 (C)	−30.497	15.435	Lu et al. (2020a)
V19-250 (PC)	core top	Atlantic	−24.1	5.8	1600	WOD Namibia 13237549 (C)	−24	5.917	Lu et al. (2020a)
V19-254 (PC)	core top	Atlantic	–23.4	8.5	1390	WOD Soviet Union 10079139 (B)	–23.22	8.42	Lu et al. (2020a)
V29-140 (PC)	core top	Atlantic	−3.1	9.3	719	WOD Congo 550522 (B)	−3.13	9.27	Lu et al. (2020a)
V29-142 (PC)	core top	Atlantic	−2.1	6.4	1017	WOD Congo 795427 (B)	−2.03	6.25	Lu et al. (2020a)
BOFS_14K (KC)	0–1	Atlantic	58.6	19.4	1756	WOD Poland 22219965 (B)	58.587	19.6	Lu et al. (2016)
ODP_1057A_1H_1A (PC)	0–2	Atlantic	32.0292	−76.0792	2595	WOD United States 676185 (B)	32 N	−76	Lu et al. (2016)
ODP_1090A_1H_1W (PC)	0–3	Atlantic	−42.9083	8.9	3702	WOD France 17901021 (B)	42.917 S	8.716	Lu et al. (2016)
ODP_1308C_1H_1A (PC)	0–3	Atlantic	49.87777	−24.23813	3871	WOD France 15607830 (B)	49.841 N	−24.106	Lu et al. (2016)
ODP_658 (PC)	0–8	Atlantic	20.74917	−18.58083	2264	WOD Japan 647227 (B)	20.713 N	−18.513	Lu et al. (2016)
RAPiD_13_9B	0–1	Atlantic	62.21183	−17.9895	1755	WOD France 16675273 (B)	62.243 N	−18.175	Lu et al. (2016)
RAPID_6_3B	0–1	Atlantic	62.06333	−16.05567	2228	WOD France 16574494 (B)	62.045 N	−16.019	Lu et al. (2016)
709A1H1W (PC)	0–1	Arabian Sea	−3.915	60.55167	3047	WOD Soviet Union 7484556 (B)	−3.58	60.48	Lu et al. (2016)

I/Ca was measured in planktonic foraminifera *T. sacculifer*, *G. bulloides*, *G. menardii*, *G. conglomerata*, *G. siphonifera*, *G. ungulata*, *P. obliquiloculata*, *G. tumida*, and *N. dutertrei* (Table 2, supplementary data). Trace element analysis was done on 6–30 foraminifera per sample, the number necessary to provide ~300 μg of carbonate material, from the 300–355 and 355–425 μm size fractions. Foraminifera crushing, chemical cleaning, and analytical procedures followed Zhou, Hess et al. (2022), a methodology that allows for simultaneous measurement of other trace elements in addition to I/Ca. Except for 4 samples of *N. dutertrei* run separately, chemical cleaning included a reductive

Table 2
Foraminifera water depth habitat and related information. Foraminifera are listed in order from shallowest to deepest dwellers. S-ETP Mg/Ca-derived calcification depths calculated using the multispecies equation of Hollstein et al. (2017). Symbiont and spinose data from Ying et al. (2023).

Species	Symbiont-bearing, spinose	ETP apparent calcification depth				Other relative habitat relationships (Boscolo-Galazzo et al., 2022)	Relative calcification depth
		S-ETP Mg/Ca-derived (range and average, this study)	**S-ETP** (Faul et al., 2000)	**Central eq. Pac.** (Watkins et al., 1996)	**N-ETP, relative to ODZ** (Davis et al., 2021)		
Globigerinoides ruber	Yes, yes	Insufficient data	0–20 m	0–70 m			Surface
Trilobatus sacculifer (without sac)	Yes, yes	5–103, ~37 m	5–25 m	0–75 m			Surface
Trilobatus sacculifer (with sac)	Yes, yes	5–75, ~22 m	5–25 m	0–75 m			Surface
Globigerina bulloides	No, yes	Insufficient data	60–105 m				Surface
Globorotalia menardii	Facultative, no	Insufficient data	45–70 m	5–45 m	Oxic through ODZ, dominantly transitional		Shallow subsurface
Globoquadrina conglomerata	No, no	5–124, ~59 m			Transitional		Shallow subsurface
Globigerinella siphonifera	Yes, yes	5–181, ~127 m			Oxic to (dominantly) transitional		Shallow subsurface
Globorotali ungulata	No, no	Insufficient data				Above *G. tumida*	Shallow subsurface
Pulleniatina obliquiloculata	Facultative, no	3–216, ~129 m	65–110 m				Deep subsurface
Globorotalia tumida	No, no	105–219, ~159 m	65–110 m				Deep subsurface
Neogloboquadrina dutertrei	Facultative, no	10–250, ~131 m	75–135 m				Deep subsurface

cleaning step. To correct for the effects of reductive cleaning, I/Ca values for samples that received this step were multiplied by 1.3 following Zhou, Hess et al. (2022) who showed that samples that were not reductively cleaned had I/Ca ratios ~30 % higher than those that were. Mg/Ca values were multiplied by 1.1 following Barker et al. (2003) who showed that reductive cleaning lowers Mg/Ca values by 10–15 %. Both corrected and uncorrected values are given in supplementary data.

Samples were analyzed on a Thermo Element XR Sector Field Inductively Coupled Plasma Mass Spectrometer in low resolution (m/Δm = 300) using the method of (Rosenthal et al., 1999). Data were corrected for matrix effects due to varying Ca concentration among samples using six standard solutions with the same elemental ratios and varying Ca concentrations. For numbers reported in the text, plus-or-minus error is 1 standard deviation. Due to the volatile nature of iodine, standard solutions were prepared the morning of each run; the RSD% from internal standards with concentrations spanning the range of foraminiferal values for I/Ca is 11–13 %, a measure of the standard deviation of the procedure, including preparation and measurement. Repeated measurements of JCp-1 coral standard, commonly used as a standard for I/Ca measurements, have an RSD of 10.24 % (4.20 ± 0.43 μmol/mol) from our lab (Zhou, Hess et al., 2022). We compare our I/Ca data with published core-top data from Lu et al. (2016, 2020a) and Zhou, Hess et al. (2022), excluding samples from deeper than 10 cm core depth because deeper samples have a greater likelihood of having been deposited under a different hydrographic regime than the modern. Lu et al. (2016, 2020a) measured I/Ca in a basic solution and without the reductive cleaning step. Zhou, Hess et al. (2022) show that I/Ca measured in an internal standard approximating foraminiferal composition and in JCp-1 coral reference material yield similar results when analyzed in a basic solution following the methods used by previous I/Ca researchers including Lu et al. (2016, 2020a) and when analyzed in an acidic solution, as done here. They further show that foraminiferal data generated in our lab using the same techniques as data presented herein are similar to data generated in other labs using the methods Lu et al. (2016, 2020a) used. Fig. S1 illustrates this, with data from 3 sites measured in our lab plotted with overlapping data from the same sites measured using a basic solution and without reductive cleaning. Paleoceanographic samples measured using our methodology have yielded observable trends in I/Ca through time, with statistically significant offsets occurring at the same time in multiple species (Hess et al., 2023).

For sites in the ETP, we determined water-depth habitats for each species using Mg/Ca data, collected alongside I/Ca data, to calculate calcification temperature for each sample, then finding the depth at which the CTD temperature profile at or near that site reaches that temperature, deemed the depth of calcification (Figs. 2, S2, Table 2). This includes sites where Zhou, Hess et al. (2022) presented I/Ca data measured using the same methodology as here and therefore had Mg/Ca data available, published here for the first time. We compare calcification temperatures calculated using the classic multi-species equation of Anand et al. (2003) ($Mg/Ca = 0.38\,e^{0.9T}$) from the North Atlantic, species-specific equations of Cléroux et al. (2008) (see their Table 3) from the North Atlantic, and the multispecies equation ($Mg/Ca = 0.26\,e^{0.097T}$) and species-specific equations of Hollstein et al. (2017) (see their Table 5) from the West Pacific warm pool.

3. Results

3.1. Foraminiferal apparent calcification depths

Mg/Ca-temperature calibrations from Anand et al. (2003), Cléroux et al. (2008), and Hollstein et al. (2017) yield similar apparent calcification depths by species for the 13 species we measured in the S-ETP (Fig. S2). We classify *G. ruber*, *T. sacculifer* and *G. bulloides* as surface calcifiers, *G. menardii*, *G. conglomerata*, *G. siphonifera*, and *G. ungulata* shallow subsurface calcifiers, and *P. obliquiloculata*, *G. tumida*, and *N. dutertrei* as deep subsurface calcifiers (Table 2). Over all, depths calculated using the Hollstein et al. (2017) multispecies equation correspond well with depths from this area derived from core-top oxygen isotopes (Faul et al., 2000) (Fig. S2), so we adopt these depths in Table 2 and Fig. 3. As the Hollstein et al. (2017) calibration is based on core-top data from the equatorial Pacific, it inherently accounts for possible dissolution effects, and our Mg/Ca values are not unreasonably low as would be expected if dissolution were a concern (e.g., Regenberg et al., 2006). We note that relative water depths hold true regardless of which calibration we choose. For deep subsurface calcifiers, our data cover a wider depth range and are generally deeper than those found by Faul et al. (2000). We note that the CTDs used to convert from temperature to depth were taken between October 28 and December 17th 2013, representing only a snapshot of temperature at each site, which could complicate the conversion from calcification temperature to depth. However, relative calcification depths are consistent with previously reported relationships from the ETP. For example, core-top

oxygen isotope data from the S-ETP agree that *T. sacculifer* calcifies relatively shallowly and *P. obliquiloculata*, *G. tumida*, and *N. dutertrei* calcify relatively deeply (Faul et al., 2000). *G. conglomerata* calcification depths are between those of *T. sacculifer* and *G. siphonifera*, consistently above those for deep-dwelling *P. obliquiloculata*, *G. tumida*, and *N. dutertrei* (Fig. 3A). While *G. conglomerata* is a deep subsurface dweller

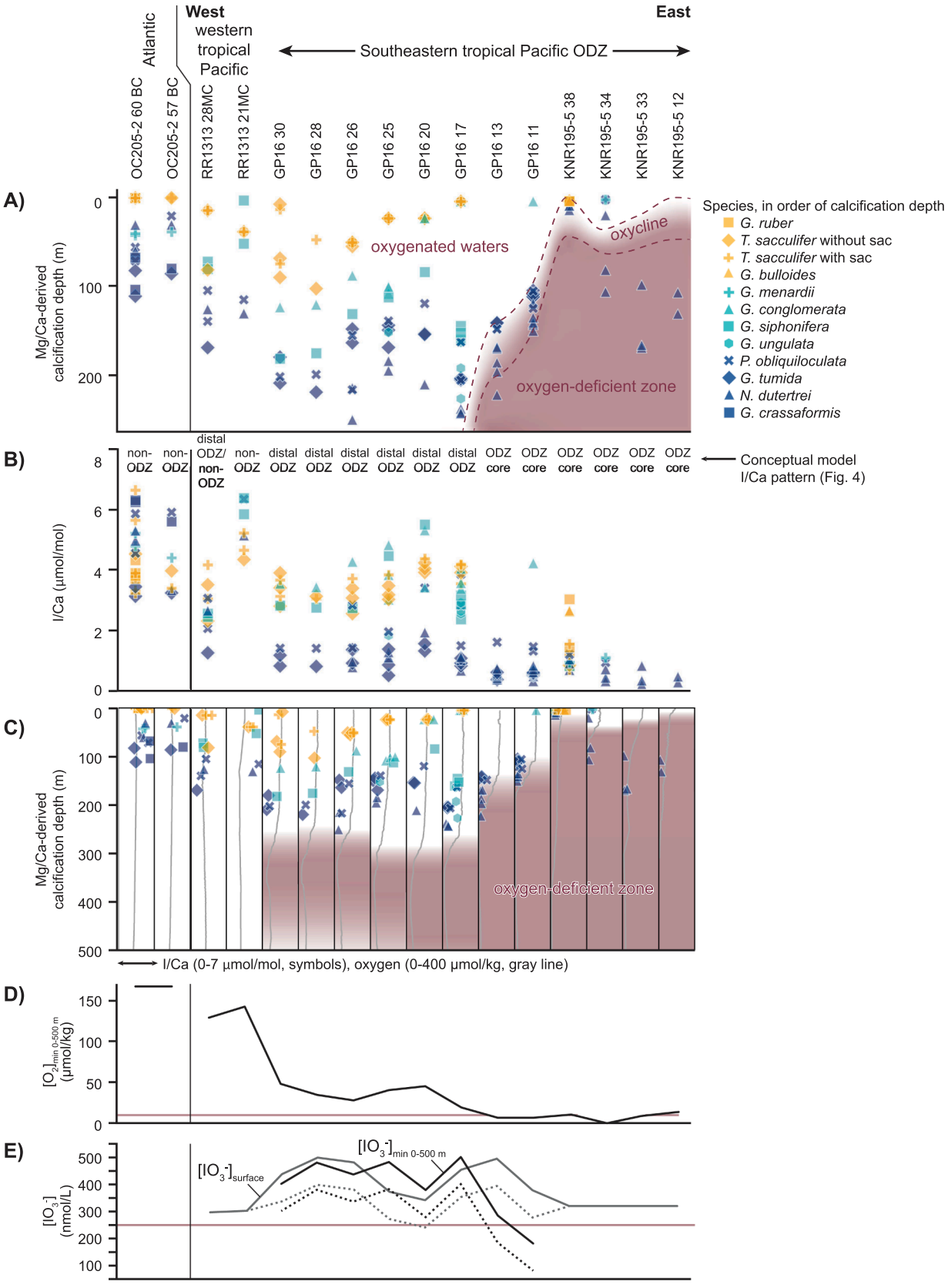

(caption on next page)

Fig. 3. Cross section through the equatorial Pacific, from the S-ETP ODZ in the east to the moderately well oxygenated West Pacific warm pool in the west. North Atlantic sites are presented for comparison. (A) Mg/Ca-derived calcification depths for each sample. Red area shows oxygen-deficient zone, based on oxycline depth from CTDs. Note that the only species apparently living in the ODZ is *N. dutertrei*. (B) I/Ca. (C) Combination of data from parts A and B, showing I/Ca (symbols) and water-column oxygenation (gray line) on the x-axis versus calcification depth on the y-axis, at each site. (D) Minimum oxygen concentration in the upper water column (0–500 m water depth). Red line indicates value of $[O_2]_{min\ 0\text{-}500m}$ below which Lu et al. (2020a) suggest iodate reduction may begin in the Pacific and Arabian Sea (10 μmol/kg). (E) Iodate concentrations. Concentrations at the surface from Cutter et al. (2018), Elderfield and Truesdale (1980), and Tsunogai and Henmi (1971), minimum concentrations at 0–500 m from Cutter (2017). Dashed line is corrected downwards by 100 nmol/L to account for differences in measurement in these samples, as per Moriyasu et al. (2023). Red line indicates threshold value used by (Lu et al., 2016) to distinguish ODZs (below, <250 nmol/L surface iodate) from non-ODZs (above, >250 nmol/L surface iodate). Note that surface iodate remains at or above the 250 nmol/L threshold throughout the S-ETP ODZ. ODZ core, distal ODZ, and non-ODZ labels are based on the I/Ca patterns from the conceptual model (Fig. 4).

in the N-ETP (Watkins et al., 1996) and western tropical Pacific (Kim et al., 2023), it has no depth preference in the Arabian Sea (Hutson, 1977; Duplessy et al., 1981) and Mg/Ca data suggest that it calcifies relatively shallowly in the S-ETP.

3.2. I/Ca

I/Ca in planktonic foraminifera has been used as a proxy for upper water-column oxygenation, particularly in ODZs to determine their strength (Zhou et al., 2014; Lu et al., 2016; Hoogakker et al., 2018; Hess et al., 2023). The I/Ca ratio is typically compared to the minimum oxygen concentration in the upper 500 m of water, which we here abbreviate as $[O_2]_{min}$ following Lu et al., (2016, 2020a) and Zhou, Hess et al. (2022). This depth encompasses the depth where oxygen is at its minimum in ODZs (Karstensen et al., 2008). We have also looked for correlations between I/Ca and other oxygenation values including the average and minimum oxygen concentration in the upper 100 m (depth occupied by surface calcifiers) and 500 m (depth including the strongest part of ODZs), and the minimum in all depths, and found the best correlation with $[O_2]_{min}$. These oxygenation numbers are provided in the supplementary data.

In the S-ETP ODZ, I/Ca is generally higher in surface and shallow subsurface calcifiers (Fig. 3B–C). The following numbers are averages from all S-ETP ODZ sites (KNR195-5 and GP16 sites). I/Ca from surface dwellers *T. sacculifer* without and with a sac are 3.33 ± 1.12 (n = 16) and 3.45 ± 1.10 μmol/mol (n = 10), respectively, from shallow subsurface dwellers *G. siphonifera* and *G. conglomerata* are 3.07 ± 1.22 (n = 9) and 3.91 ± 0.63 μmol/mol (n = 12), respectively. Deep subsurface calcifiers *P. obliquiloculata*, *G. tumida*, and *N. dutertrei* have I/Ca of 1.87 ± 1.45 (n = 15), 0.92 ± 1.38 (n = 19), and 0.75 ± 0.89 μmol/mol (n = 21), respectively. Traversing the ODZ, I/Ca values in all foraminiferal species are lowest in the east, in the core of the ODZ (Fig. 3B), where both the minimum oxygen concentration and minimum iodate concentration in the upper 500 m of the water column are lowest (Fig. 3D–E). In surface and shallow-subsurface species, I/Ca values are higher in the distal ODZ, reaching their highest values of nearly 6 μmol/mol where the ODZ is deepest (GP16 Sites 17, 20, and 25). In deep subsurface species, I/Ca values are generally < 2 μmol/mol (Fig. 3B).

Comparing the core of the ODZ (KNR195-5 sites and GP16 Sites 11–13, $[O_2]_{min}$ < 14 μ mol/kg) to those in the distal ODZ (GP16 Sites 17–30, $[O_2]_{min}$ ~20–50 μmol/kg), I/Ca values are statistically lower in the ODZ core. *T. sacculifer* values rise from an average of 1.11 ± 0.32 μmol/mol (n = 4) in the ODZ core to ~3.59 ± 0.49 μmol/mol (n = 24) in the distal ODZ (statistically different with a p-value of $8.27x10^{-5}$). *P. obliquiloculata* values rise from ~1.21 ± 0.35 μmol/mol (n = 6) in the ODZ core to ~2.31 ± 0.89 μmol/mol (n = 9) in the distal ODZ (p-value 0.01), and *G. tumida* values rise from ~0.58 ± 0.08 (n = 6) to ~1.08 ± 0.28 μmol/mol (n = 13) (p-value $4.28x10^{-5}$). One exception is *N. dutertrei*, the deepest calcifying species, which has very low values across the ODZ (~0.60 ± 0.22 μmol/mol (n = 21) in the ODZ core and ~0.36 ± 0.36 μmol/mol (n = 8) in the distal ODZ). *N. dutertrei* has been shown to calcify in the microenvironment of marine organic aggregates (Fehrenbacher et al., 2018), which are oxygen-depleted (Alldredge and Cohen, 1987). However, I/Ca values from this species are relatively high in non-ODZ settings (~3.90 ± 1.66 μmol/mol (n = 2) in the western tropical Pacific and ~4.53 ± 0.85 μmol/mol (n = 3) in Atlantic Ocean sites with $[O_2]_{min}$ > 100 μmol/kg), suggesting that I/Ca values are primarily driven by ambient conditions rather than aggregate microenvironments.

Sites RR1313 21MC and 28MC in the western tropical Pacific have intermediate oxygenation, $[O_2]_{min}$ of 142 and 129 μmol/kg, respectively, and have I/Ca values similar to or above those in the distal S-ETP ODZ (Fig. 3B). At these sites, I/Ca values from deep subsurface calcifiers converge with and even surpass values from surface dwellers. For example, even the deepest dwelling *N. dutertrei* has I/Ca of 5.13 and 2.66 μmol/mol at Sites 21MC and 28MC, respectively. Nearby Site RR1313 2MC has slightly lower oxygenation ($[O_2]_{min}$ = 105 μmol/kg) but exceptionally low I/Ca values (1.06–2.37 μmol/mol) for an area with intermediate oxygenation. Immediately north of this site is a small, restricted basin between Papua New Guinea and the D'Entrecasteau Islands where oxygenation is less than in surrounding waters (Boyer et al., 2018). We infer that this site is bathed by low-oxygen waters, resulting in the observed low I/Ca ratios. Lu et al. (2020a) report similarly low values at shallow water sites (most <~500 m water depth) near the southern tip of Africa where oxygen concentrations are highly variable over small spatial scales. They excluded those data from their global calibration because they appear to be affected by local oxygen variability not captured in oxygenation data measured at those sites, and we do the same with that data and our data from Site RR1313 2MC (starred entries in Table 1).

At intermediate-oxygenation ($[O_2]_{min}$ = 169 μmol/mol) Sites OC205-2 57BC and 60BC in the North Atlantic, I/Ca values are higher overall than in the S-ETP ODZ, with values ranging from 3.15 to 6.63 μmol/mol (Fig. 3B). They follow a similar pattern to those from the western tropical Pacific, with I/Ca from deep subsurface calcifiers generally exceeding that in surface species.

4. Discussion

To better understand what controls the observed I/Ca values, we first discuss the distribution of iodate and iodide in the oceans in relation to oxygenation and primary productivity and consider where foraminifera calcify with respect to that distribution. We use a regional transect through the equatorial Pacific to build a conceptual model explaining how this iodate distribution affects foraminiferal I/Ca (Fig. 4). We then place our new data in a global context encompassing the full range of oxygenation and I/Ca values found globally and build an I/Ca-oxygenation correlation. Finally, we discuss how I/Ca can be used on regional and global scales to reconstruct paleo-oxygenation in the geologic past.

4.1. Foraminiferal apparent calcification depths in the S-ETP ODZ

The distribution of foraminiferal calcification depths in the S-ETP ODZ appears to respond to the depth of the ODZ, with calcification compressing into shallower waters eastward where the ODZ is shallow (Fig. 3A), with one exception. Westward, in the distal ODZ (GEOTRACES GP16 sites 30 through 17), foraminifera calcify from the surface down to ~250 m. Eastward, where the oxycline and thermocline shallow to <250 m, calcification depths follow the oxycline/thermocline,

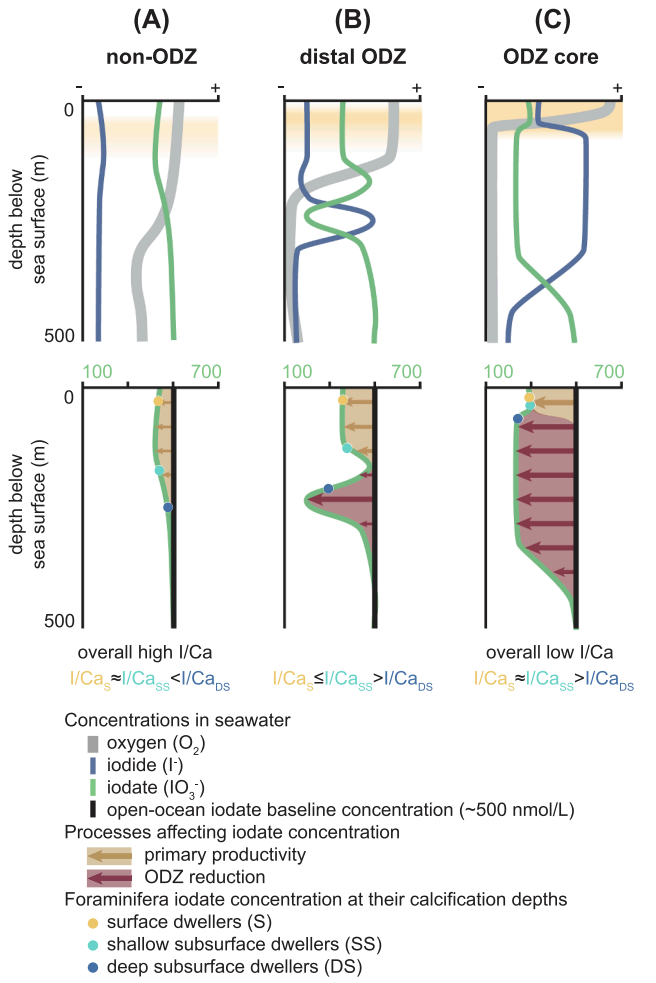

Fig. 4. Conceptual model for water-column iodate concentrations based on the S-ETP ODZ. Upper panels show oxygen (gray), iodate (green), and iodide (blue) concentrations in the upper water column including the upper part of an ODZ. Yellow shaded area indicates primary productivity. Lower panels show factors affecting iodate concentration. Black line indicates baseline open-ocean iodate concentration and arrows and shading indicate factors causing loss of iodate and deviation from that baseline value. Expected relationship between I/Ca values in foraminifera calcifying in different water depths is noted below each part. Note that though iodate concentrations are non-zero in the S-ETP ODZ, they reach zero in other ODZs, though relative patterns of concentrations hold true.

compressing into the mixed layer in the upper 10s of meters of the water column to the east, where the ODZ is strongest. Species remain in the oxygenated water column, with one notable exception. *N. dutertrei* appears to calcify within the ODZ, at depths where oxygen concentrations reach <8 μmol/kg (Fig. 3A). Crusts formed by *N. dutertrei* tend to lower their Mg/Ca ratios, which would lead to falsely cold apparent calcification temperatures (Jonkers et al., 2012). However, calculated depths are consistent with observations from this area made by Faul et al. (2000), who noted that in the core of the ODZ, *N. dutertrei* calcify deeper, with depths diverging from those occupied by *G. tumida*. Our calcification depths for *N. dutertrei* are also consistent with those found by Faul et al. (2000) (60–160 m) and Kalansky (2014) (100–130 m). In the N-ETP ODZ, *Globorotaloides hexagonus* live in severely hypoxic waters (<22 μM oxygen)(Davis et al., 2021). Though *N. dutertrei* are rare in that study, our results suggest that it may fill a similar niche in the S-ETP ODZ as *G. hexagonus* does in the N-ETP ODZ. Further investigation using plankton-tow data are needed to test this hypothesis.

4.2. Iodate distribution in the oceans

Ocean iodate data are limited, with most data being surface iodate concentrations (e.g., Chance et al., 2014). Water-column data are scarce, not available at all sites with I/Ca data, so a direct comparison globally may be incomplete. However, transects across the ETP ODZ (Cutter et al., 2018; Moriyasu et al., 2020) and in the North Pacific (Moriyasu et al., 2023) show the lateral variability through the ODZ and in the open ocean. Data from the Atlantic, Indian, and Southern Oceans (Jickells et al., 1988; Rue et al., 1997; Farrenkopf et al., 1997; Campos et al., 1999; Farrenkopf and Luther, 2002; Bluhm, 2010; Chance et al., 2010; Bluhm et al., 2011) provide a sufficiently global view.

In the deep ocean (>1000 m), iodine exists almost entirely as iodate, with concentrations near 500 nmol/L (e.g., Cutter et al., 2018; Farrenkopf et al., 1997; Wong and Brewer, 1977). The factors controlling iodate distribution in the upper ocean, however, are complex, related to productivity and redox reactions in the water and seafloor sediments (Fig. S3), and they are an area of active study (Wadley et al., 2020; Moriyasu et al., 2023; Luther, 2023; Cheng et al., 2024; Evans et al., 2024). While anoxic seafloor sediments that ODZ waters impinge upon are an important source of iodine in ODZs, it is in the form of iodide due to the extremely low oxygen concentration in these sediments (Cutter et al., 2018; Moriyasu et al., 2020) and is likely not a major source of iodate, the species affecting the I/Ca proxy (Cheng et al., 2024). Thus, to a first order, low iodate concentrations in open-ocean shallow waters where planktonic foraminifera calcify are the result of primary productivity in the mixed layer and, where present, low oxygen concentrations in underlying ODZs.

Outside of ODZs, the effect of primary productivity is the dominant factor causing iodate concentrations to deviate from the open-ocean baseline value of ~500 nmol/L, resulting in less iodate and more iodide above the thermocline than below (Chance et al., 2010; Moriyasu et al., 2023) (Fig. 4A). Absent a sedimentary source of iodide, iodide concentrations correlate positively with the amount of productivity (Chance et al., 2010). A range of phytoplankton groups are involved in iodate reduction, including diatoms, coccolithophores, and phaeocystales (Chance et al., 2007; Hepach et al., 2020). There is a lag between iodate uptake and release of iodide later in the lifecycle, and iodate reaches its minimum when fluorescence (reflects the concentration of Chlorophyll-A, which is an indicator of phytoplankton productivity) reaches its maximum (Hepach et al., 2020). Thus, the time of greatest productivity coincides with the lowest iodate concentrations in the mixed layer. The effect of productivity on iodate concentrations can be seen in the mixed layer of the equatorial Pacific water-column data, where increased fluorescence indicates high biomass in the zone of primary productivity (Fig. 2).

In areas with ODZs, iodate concentrations in the mixed layer are low (Lu et al., 2020a, and references therein), unsurprising since these are highly productive areas (Engel et al., 2022). Concentrations are even lower in the ODZ, with an iodate minima and iodide maxima below the thermocline (Cutter et al., 2018; Farrenkopf et al., 1997; Farrenkopf and Luther, 2002; Moriyasu et al., 2020; Rue et al., 1997) (Fig. 4B–C). In the absence of oxygen, iodate converts to iodide and Moriyasu et al. (2020) found iodate to be completely absent in some profiles in the N-ETP ODZ where oxygen was not detected. Iodate has a Gibbs free energy for organic-matter decomposition between that of nitrate and Mn(IV), making it a favorable electron acceptor for microbial reduction of organic matter in ODZs (Farrenkopf et al., 1997; Farrenkopf and Luther, 2002). It can also be reduced abiotically in the presence of some species of iron and sulfur (Councell et al., 1997). Iodate loss in the ODZ is also felt in the overlying mixed layer, where iodate concentrations are too low to be explained exclusively by primary production (Cheng et al., 2024).

In the S-ETP ODZ, the subsurface zone of iodate reduction is above ~450 m water depth, is thickest near the continent, and shallows and thins westward (Fig. 2 green shaded area) (Cutter et al., 2018). In

easternmost sites, iodate falls from a background value of ~500 nmol/L below ~450 m to < 200 nmol/L in the uppermost ODZ and iodide increases from background values of ~100 nmol/mol below ~450 m to > 1100 nmol/L in the uppermost ODZ. The minimum iodate concentration appears to vary by ODZ. Though iodate is completely reduced in the N-ETP ODZ, with concentrations falling below detection limits (Rue et al., 1997; Moriyasu et al., 2020), iodate concentrations are higher in the S-ETP and do not reach zero even in the most oxygen-depleted part of the ODZ (Cutter et al., 2018; Moriyasu et al., 2023). Moriyasu et al. (2023) suggested this is an analytical artefact, attributing it at least in part to the gas used to purge oxygen interference during measurement. They found ~100 nmol/L higher iodate concentrations when N_2 gas was used, as by Cutter et al. (2018) for measurements at GP16 sites in the southern lobe, compared to Ar gas, as used by Moriyasu et al. (2023) in the northern lobe. There is also a 5 year time gap between collection of the two datasets. Surface iodate concentration in GP16 sites is ~363 nmol/L (upper 100 m, average for GP16 Sites 1–13) (Fig. 2); correcting these downwards by ~100 nmol/L to account for the difference in measurement methodology results in similar values as in the northern lobe of the ODZ (~250 nmol/L) (Lu et al., 2016; Moriyasu et al., 2023). However, within the ODZ, minimum iodate concentrations are ~249 nmol/L (minimum in the upper 500 m, average for GP16 Sites 1–13) (Fig. 2); even after correction for different analytical techniques, minimum iodate concentrations in the ODZ do not reach zero as in the N-ETP ODZ. As noted by Moriyasu et al. (2020), waters in the N-ETP ODZ are ~30 years older than those in the S-ETP (Karstensen et al., 2008), and the additional 30 years may have been necessary for complete iodate reduction in the N-ETP. Differences in iodate reduction rate have also been found between the N-ETP and Arabian Sea ODZs, and slower iodate reduction may contribute to higher iodate concentrations in the S-ETP (Hardisty et al., 2021).

4.3. I/Ca ratios follow patterns of iodate distribution

A conceptual model for water-column oxygenation and iodate distribution and predicted I/Ca values is shown in Fig. 4 and is based on data from the equatorial Pacific (Figs. 2 and 3). Water-column properties are taken from GP16 Sites 4–9 (“ODZ core”), Sites 11 and 13 (“distal ODZ”) and Sites 15–36 (“non-ODZ”) (Cutter, 2017; Moffett et al., 2020). At well-oxygenated sites from non-ODZ areas, iodate concentrations are lowest in the mixed layer due to the effect of primary productivity (Chance et al., 2010; Moriyasu et al., 2023). As a result, I/Ca values are expected to be relatively high overall, with the highest values in deep-subsurface calcifying foraminifera, furthest removed from the zone of primary productivity (Fig. 4A). At sites in the core of the ODZ, iodate concentrations in the mixed layer are relatively low and below the thermocline and oxycline are even lower, owing to the combined effects of high productivity at the sea surface and the remineralization of organic matter under low-oxygen conditions in the ODZ (Cutter et al., 2018; Farrenkopf et al., 1997; Farrenkopf and Luther, 2002; Moriyasu et al., 2020; Rue et al., 1997). As a result, I/Ca values are expected to be low in all species of foraminifera and lowest in deep-calcifying species (Fig. 4C). In distal-ODZ settings, where the thermocline and oxycline deepen and the low-oxygen interval thins, the zones of low iodate in the mixed layer and below the thermocline separate. This results in the lowest I/Ca values in deep subsurface calcifiers affected by the subsurface low-iodate zone and moderately high I/Ca values in surface and shallow-subsurface calcifiers. Shallow subsurface calcifiers that live in the interval between surface and subsurface low-iodate zones may have the highest I/Ca values (Fig. 4B).

The patterns of I/Ca distribution predicted by the conceptual model can be seen in the measured I/Ca data, however, it appears that the S-ETP ODZ I/Ca data were emplaced during a time when the ODZ was expanded relative to that documented in the water-column iodate concentration data. Throughout the GP16 sites, I/Ca values are lowest in deep-subsurface calcifiers, which is inconsistent with the apparent absence of a low-iodate zone in westward Sites 15–36 based on water-column data (Fig. 2). One possibility is a species effect on I/Ca concentrations. However, the low I/Ca values are not limited to a single species and values are lower for species calcifying progressively deeper in the water column. Also, these same species in other areas have higher I/Ca values and values higher than more shallowly calcifying species (Fig. 3B). Therefore, we infer that there was a subsurface low-iodate zone when those foraminifera were calcifying, which is not captured in the GP16 water-column data. The water-column iodate data present a snapshot of the water-column properties, not capturing variability on seasonal and longer timescales. By contrast, our core-top sediments, from the upper 1–4 cm of sediment, likely encompass hundreds to a few thousands of years of deposition (e.g., Bender et al. (1971) found sedimentation rates of 0.45–1.50 cm/kyr at nearby sites). The S-ETP ODZ expands significantly under La Niña conditions (Helly and Levin, 2004). Temperature and precipitation patterns suggest that the tropical Pacific experienced more La Niña-like conditions during the Medieval Warm Period (~1000–1300 CE) (Cobb et al., 2003; Mann et al., 2009; Zhang et al., 2022; Jiang et al., 2023), which could easily be encompassed by core top samples. We therefore infer that the foraminifera from our GP16 samples lived during a time when La Niña-like conditions were more prevalent and the ODZ was expanded. We note, however, that the Mg/Ca-derived sea-surface temperatures from the S-ETP ODZ were similar during the Medieval Warm Period and in the modern (<1°C difference) (Rustic et al., 2015), suggesting that our Mg/Ca-derived calcification depths are likely still accurate.

Despite the above caveats, a pattern in the I/Ca data emerges, as laid out in the conceptual model (Fig. 4), and the designations as “ODZ core,” “distal ODZ,” and “non-ODZ” used in Fig. 3 are based on I/Ca patterns within and among species as shown in Fig. 4. Some variability is expected because foraminifera calcify over a range of depths, even within one species (Fig. 3A; Watkins et al., 1996; Faul et al., 2000; Hollstein et al., 2017) and lumping foraminifera species into shallow, shallow subsurface, and deep subsurface is a simplification of this natural variability. The expected non-ODZ I/Ca distribution, with overall high I/Ca values and I/Ca for deep subsurface calcifiers among the highest, is present in our intermediate-oxygenation sites in the western tropical Pacific and Atlantic (Sites RR1313 21MC, OC205-2 57 BC and 60 BC; Fig. 3B) and sites from Lu et al. (2020a) in the well-oxygenated Atlantic Ocean (Fig. 5A). The ODZ-core pattern, with overall low I/Ca values and I/Ca for deep subsurface calcifiers being lowest, is apparent in low-oxygen areas in the S-ETP ODZ. In KNR195-5 sites, I/Ca from deep-calcifying species are the lowest of all sites in the equatorial Pacific transect, and in sites where species from multiple depths are present (KNR195-5 Sites 34 and 38) values from deep-calcifying species are typically lowest, though there is overlap due to the generally low I/Ca values in all species. This is also true for low-oxygen sites from the eastern tropical Atlantic (Lu et al., 2020a). Data from GP16 Sites 11 and 13 are restricted to deep-calcifiers, with the exception of one *G. conglomerata* point, and generally low I/Ca values in *G. tumida* suggest they follow the ODZ-core pattern. At GP16 Sites 17–30, I/Ca values spread out, values from deep subsurface calcifiers are generally lowest, and at Sites 20 and 25, where the oxycline is deepest, shallow subsurface I/Ca values rise above surface values, consistent with a distal ODZ-type pattern.

4.4. Toward a global I/Ca-oxygen calibration

A positive correlation between I/Ca and $[O_2]_{min}$ is apparent for data from all species and for species that calcify at particular depths (Fig. 5). Though earlier datasets appeared to operate on a threshold system (Lu et al., 2016; 2020a), much of the new data presented here and in Zhou, Hess et al. (2022) fall outside of those thresholds (Fig. S4). Most surface and shallow subsurface I/Ca values from the S-ETP are > 2.5 μmol/mol, despite the low oxygen concentrations ($[O_2]_{min}$ < 70 μmol/kg) in that area. Some data from Sites RR1313 28MC and OC205-2 57B and 60BC

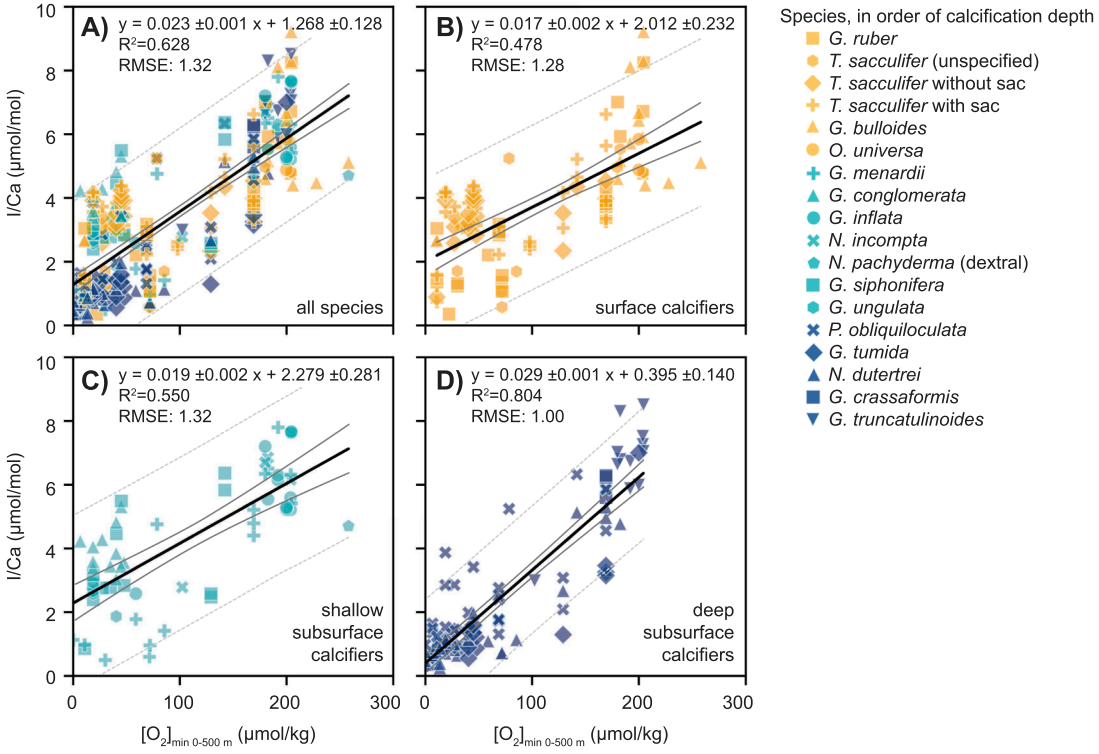

Fig. 5. I/Ca in core-top planktonic foraminifera versus minimum oxygen concentration in the top 500 m of the water column. Sites are those without highly variable local oxygen (excluding data from starred sites in Table 1), including all data from the top ~10 cm of sediment. Includes new data and existing data from Lu et al. (2016; 2020a) and Zhou, Hess et al. (2022) (Fig. S5). Black lines are ordinary least squares regressions, with 95 % confidence interval on the line as represented in the equation for the line in dark gray and 95 % prediction interval in dashed light gray. (A) All species. This plot is comparable to Fig. 2a in Lu et al. (2016) and Fig. 5c-d in Lu et al. (2020a). (B) Surface calcifiers. (C) Shallow subsurface calcifiers. (D) Deep subsurface calcifiers.

are < 2.5 despite $[O_2]_{min}$ > 100 µmol/kg. In the new dataset, a clear binary threshold system is not apparent. However, in this dataset with significant scatter, it may be helpful to use cutoffs to interpret I/Ca values on the very high or very low end of the spectrum. For example, I/Ca > 4.5 µmol/mol occurs almost entirely at sites with $[O_2]_{min}$ > 140 µmol/kg, I/Ca < 3 µmol/mol occurs only at sites with $[O_2]_{min}$ < 140 µmol/kg, and I/Ca < 2 µmol/mol occurs almost entirely at sites with $[O_2]_{min}$ < 90 µmol/kg.

We have tested three regression models, namely linear, break point analysis, and threshold analysis. We also tested quadratic and exponential regressions, which yield R^2 values the same or lower than that for a linear regression (R^2_{linear} = 0.63, $R^2_{quadratic}$ = 0.63, $R^2_{exponential}$ = 0.62). Bearing in mind the complexity of the iodate-oxygen-I/Ca system as described above and lacking a conceptual reason why the proxy would operate on thresholds or breakpoints, we adopt a linear model as the most parsimonious characterization of the data (Fig. 5). The 95 % confidence intervals (dark gray lines, Fig. 5) reflect how well constrained the linear regression line is and are quite tight around the line. The prediction intervals (light gray dashed lines, Fig. 5) reflect the variability in the data and are much broader. Considering the complexity of the distribution of iodate through the water column and spatially, and the depths at which foraminifera calcify with respect to that distribution, the relationship between I/Ca and $[O_2]_{min}$ is also complex. It appears that some of the large scatter in the I/Ca data (Fig. 5A) is related to this complexity. Also, the data in the compiled global dataset come from a variety of core types, from multi-corer cores where the sediment–water interface is likely to be preserved, to piston and gravity cores where it likely is not (Table 1). Part of the scatter may result from some samples being deposited at less recent times, e.g., thousands of years ago, possibly under different water-column conditions. Also, the water-column oxygenation data are a snapshot in time, not accounting for variability on seasonal or longer timescales. It is also possible that as more data become available regional calibrations might be more appropriate. However, in open-ocean settings the range of oxygen concentrations in a given region is limited; for example, sites from the GP16 transect with carbonate preservation span $[O_2]_{min}$ of 6.8–47.7 µmol/kg, only a portion of the spread from 0 to ~350 µmol/kg found globally. Thus, we use a global dataset to establish a first-order calibration.

The pattern of I/Ca values being higher in surface dwellers in low-oxygen areas (ODZs) and higher in deep subsurface dwellers in areas with more oxygen becomes even more apparent when considering the global dataset. Consistent with the conceptual model, the correlation for deep subsurface species has a steeper slope, lower y-intercept, narrower error bars, and stronger correlation (R^2 = 0.804) than that for surface or shallow subsurface species. It is logical that the y-intercept is > 0 for surface and shallow subsurface calcifiers that live above the ODZ, where iodate concentrations never reach zero. The y-intercept for deep subsurface calcifiers is nearly zero because some ODZs achieve complete iodate reduction. The slope is steepest for deep subsurface calcifiers because they are most sensitive to the presence of an ODZ, being within or immediately above ODZs where they exist, and being farthest removed from mixed layer primary productivity where they do not. This suggests that, while I/Ca of surface and shallow subsurface calcifiers does correlate with oxygenation, deep subsurface calcifiers are the most sensitive.

Zhou et al. (2014) proposed that the difference between I/Ca in surface and deep dwellers (here termed $\Delta I/Ca_{DS\text{-}S}$) could be used to identify ODZs, and they and Hoogakker et al. (2018) used these types of differences to interpret downcore trends. The global dataset now available makes it possible to quantify that relationship (Fig. 6A). Data from both the Pacific and Atlantic follow this pattern, with lower oxygen areas (<100 µmol/kg) having $\Delta I/Ca_{DS\text{-}S}$ values < 0. However, at extremely low oxygen concentrations such as in the core of the S-ETP

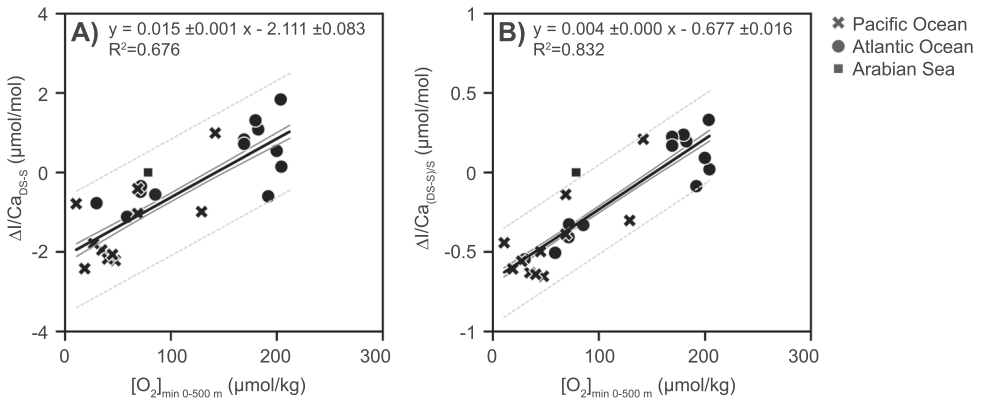

Fig. 6. I/Ca difference plots for foraminifera species from different water depths versus minimum oxygen concentration in the top 500 m of the water column. Each point represents one site, with values calculated from average I/Ca of surface calcifiers (S) and average I/Ca of deep subsurface calcifiers (DS). Black lines are ordinary least squares regressions, with 95 % prediction interval in dark gray and 95 % prediction interval in dashed light gray. (A) Difference in I/Ca between deep subsurface and surface calcifiers. (B) Difference in I/Ca between deep subsurface and surface calcifiers divided by I/Ca in surface calcifiers.

ODZ, I/Ca values are lower for all species and $\Delta I/Ca_{DS\text{-}S}$ therefore approaches 0, making a linear correlation inappropriate for extremely low-oxygen ODZ settings. To account for this, we divide by the I/Ca values in surface species to generate a $\Delta I/Ca_{(DS\text{-}S)/S}$ value, which correlates well with $[O_2]_{min}$ ($R^2 = 0.832$) (Fig. 6B). This correlation is better than that for individual I/Ca values from all species and $[O_2]_{min}$ ($R^2 = 0.628$) and similar to that for deep calcifiers ($R^2 = 0.804$) (Fig. 5). Therefore, it appears that, when multiple species are available, the best reconstruction of $[O_2]_{min}$ may be obtained in this way, using I/Ca measurements in surface and deep-subsurface calcifiers. Caution is appropriate when dealing with extinct species where calcification depth is less well constrained. This correlation might also be weaker during past warm periods, when foraminifera calcification depths may compress towards the surface (Boscolo-Galazzo et al., 2021).

4.5. Implications for paleo-oxygenation reconstruction

The above calibrations are most appropriately applied to interpret data like those used to construct them, from open-ocean settings without local variability. For example, they are not appropriate for interpreting data from restricted basins or broad, shallow shelves where waters may not mix efficiently with the open ocean. In applying the above calibrations, the large scatter in the I/Ca data must be acknowledged and they are most effective in differentiating ODZ from non-ODZ areas. This type of interpretation is straightforward in cases where I/Ca values are very high (i.e., >4.5 μmol/mol indicating $[O_2]_{min}$ > 140 μmol/kg) or very low (i.e., <2 μmol/mol indicating $[O_2]_{min}$ < 90 μmol/kg) or a shift between these two extremes is observed. For example, Hess et al. (2023) showed an I/Ca shift in the eastern tropical Pacific from ~4.9 μmol/mol during the Miocene Climatic Optimum to < 2 μmol/mol during the cooling that followed. I/Ca values > 4.5 μmol/mol during the climatic optimum support their interpretation of high oxygen concentrations at that time, and very low values support ODZ-like conditions developing during the cooling.

There is also some indication that the proxy may also be used to qualitatively track relative changes in oxygenation, when changes in I/Ca are relatively small (e.g., <1 μmol/mol) but there is a clear trend in consecutive samples (e.g., increasing, decreasing, or a step change). Though the global calibration has a wide 95 % prediction interval (light gray dashed bands in Fig. 5), I/Ca distributions in the S-ETP ODZ suggest that I/Ca can be used in the paleo record to reconstruct relatively small oxygen changes if it is possible to control for factors contributing to the variability in the global compilation. This might be accomplished by looking at records from within individual ODZs, where variability from factors that might vary globally (e.g., continental sources of iodate) is likely minimal, and by comparing records from individual foraminiferal species. In the S-ETP ODZ, we have shown that for individual species with sufficient data spanning the ODZ (*T. sacculifer*, *P. obliquiloculata*, and *G. tumida*), I/Ca values are statistically lower in the core of the ODZ compared to in distal-ODZ sites. Sites following the "ODZ core" type distribution have $[O_2]_{min}$ < 14 μ mol/kg and those following the "distal ODZ" type have $[O_2]_{min}$ ~20–50 μmol/kg (Fig. 3). This means that we can detect a change of < 36 μmol/kg oxygen, from at most 50 to less than 14 μmol/kg. If the I/Ca values were emplaced when the ODZ was more expanded than today, as we suspect, this shift would be associated with an even smaller change in oxygen concentrations. Since we can differentiate ODZ core and distal ODZ settings using I/Ca data in the S-ETP ODZ transect in species-specific data, it seems reasonable that downcore I/Ca data can also be used to detect relatively small shifts in oxygenation locally, i.e., on the order of 10s of μmol/kg shifts in $[O_2]_{min}$ at individual sites or at sites from the same ODZ. We note that this assertion is based on data from individual species comparing I/Ca values from core-ODZ sites to that in distal-ODZ sites; among different species, there is considerable spread in the I/Ca values. Therefore, relatively small shifts in I/Ca can be interpreted for paleo-records generated from individual species within the same ODZ, but not necessarily for records where multiple species are used. Results can be confirmed using additional paleo-redox proxies.

Where data from surface and deep subsurface calcifiers are available, the more precise ΔI/Ca correlation from Fig. 6B can be applied. It can be most confidently applied to more recent time periods when extant species with known water depth habitats are available. It has been suggested that foraminifera calcified more shallowly in the geologic past, reaching modern-like distributions in the Late Miocene (Boscolo-Galazzo et al., 2021, 2022), so we urge caution in applying the ΔI/Ca approach to older samples. However, a similar approach has been successfully used to interpret samples as old as the Paleocene-Eocene thermal maximum (Zhou et al., 2014), giving promise to its potential even in older samples.

5. Conclusions

Globally, I/Ca values in planktonic foraminifera are positively correlated with $[O_2]_{min}$. I/Ca > 4.5 μmol/mol indicates $[O_2]_{min}$ > 140 μmol/kg, I/Ca < 3 μmol/mol indicates $[O_2]_{min}$ < 140 μmol/kg, and I/Ca < 2 μmol/mol indicates $[O_2]_{min}$ < 90 μmol/kg. A linear relationship is made apparent by new data from areas with intermediate oxygen concentrations (100–170 μmol/kg). This relationship varies for species that calcified at different water depths, with deep subsurface species being the most sensitive to minimum oxygen concentrations. In well-oxygenated areas, iodate concentrations are lowest in the mixed layer, the result of iodate reduction by primary producers. As a result, I/Ca

values are lowest in surface calcifiers and highest in deep subsurface species that calcified farthest from the zone of primary productivity. In ODZs, iodate concentrations are lowest in the ODZ, where iodate is used in lieu of oxygen to respire organic matter, and are also low in the mixed layer due to high primary productivity and proximity to the shallow ODZ. As a result, I/Ca values are low in all species and lowest in deep subsurface calcifiers. In the distal ODZ iodate concentrations are overall higher than in the core of the ODZ, with values lowest in deep subsurface calcifiers who lived closest to the ODZ. The difference in I/Ca values between deep subsurface and surface calcifiers can therefore be used to predict oxygenation. We find the best correlation to $[O_2]_{min}$ when this difference is normalized to surface I/Ca values, thus accounting for both the relationship between surface and deep dwellers and the overall positive correlation between I/Ca and $[O_2]_{min}$.

That these trends in I/Ca can differentiate areas in the core of the S-ETP ODZ with $[O_2]_{min} < 14$ μmol/kg from more distal areas with ~20–50 μmol/kg suggests that in paleoceanographic studies from individual ODZs, I/Ca from single species may be able to detect small relative changes in oxygenation on the order of 10s of μmol/kg. We urge caution in applying the proxy to areas with oxygen variability over small distances, such as in shallow water (i.e., <500 m water depth) near continents or near restricted basins. Results can be confirmed by applying a multiproxy approach, and when the other proxy operates at different oxygenation levels a more complete picture of oxygenation changes through time can be built (e.g., Hess et al., 2023).

CRediT authorship contribution statement

Anya V. Hess: Writing – review & editing, Writing – original draft, Visualization, Validation, Project administration, Methodology, Investigation, Funding acquisition, Formal analysis, Data curation, Conceptualization. **Yair Rosenthal:** Writing – review & editing, Supervision, Resources, Methodology, Funding acquisition, Conceptualization. **Xiaoli Zhou:** Writing – review & editing, Investigation, Funding acquisition. **Kaixuan Bu:** Investigation.

Declaration of competing interest

The authors declare that they have no known competing financial interests or personal relationships that could have appeared to influence the work reported in this paper.

Acknowledgements

Funding for this project was provided by the Cushman Foundation for Foraminiferal Research through a Johanna M. Resig Foraminiferal Research Fellowship for A.V.H and NSF grant OCE-1834208 to Y.R. This work is supported by the National Natural Science Foundation of China (42006053) and the National Key Research and Development Program of China (2021YFF0502500) to X.Z. Thank you to Dr. Martin Fleisher and the GEOTRACES program for supplying samples, as well as scientists from the other cruises whose samples were vital to this work. We thank Lois Merritt for her help with sample preparation. We thank Dr. Rosy Chance for her thoughts regarding ocean iodate concentrations and help locating iodate concentration data. Thank you to Drs. Delia Oppo, Kassandra Costa, and Jake Gebbie for their mentorship and insights regarding this work.

Appendix A. Supplementary material

Supplementary figures S1–S5 containing information comparing I/Ca results from analyses using different methodologies, foraminiferal calcification depths from Mg/Ca, water column data (oxygen, iodide, and iodate) from eastern equatorial Pacific GEOTRACES GP16 sites, and plots of I/Ca versus $[O_2]_{min}$ highlighting data that fall outside of previous thresholds, new and existing data, and data distribution by basin. Supplementary material to this article can be found online at https://doi.org/10.1016/j.gca.2025.01.018.

Data availability

Data are available through Zenodo at https://doi.org/10.5281/zenodo.11068119.

References

Alldredge, A.L., Cohen, Y., 1987. Can microscale chemical patches persist in the sea? Microelectrode study of marine snow, Fecal Pellets. *Science* 235, 689–691.
Anand, P., Elderfield, H., Conte, M.H., 2003. Calibration of Mg/Ca thermometry in planktonic foraminifera from a sediment trap time series: Calibration of Mg/Ca thermometry in planktonic foraminifera. *Paleoceanography* 18 (28–1), 28.
Auderset, A., Moretti, S., Taphorn, B., Ebner, P.-R., Kast, E., Wang, X.T., Schiebel, R., Sigman, D.M., Haug, G.H., Martínez-García, A., 2022. Enhanced ocean oxygenation during Cenozoic warm periods. *Nature* 609, 77–82.
Barker, S., Greaves, M., Elderfield, H., 2003. A study of cleaning procedures used for foraminiferal Mg/Ca paleothermometry. *Geochem. Geophys. Geosyst.* 4.
Bender, M., Broecker, W., Gornitz, V., Middel, U., Kay, R., Sun, S.-S., Biscaye, P., 1971. Geochemistry of three cores from the East Pacific Rise. *Earth Planet. Sci. Lett.* 12, 425–433.
Bluhm, K., 2010. The influence of marine phytoplankton on iodine speciation in the Tropical and Southern Atlantic Ocean. Christian-Albrechts-Universität.
Bluhm, K., Croot, P.L., Huhn, O., Rohardt, G., Lochte, K., 2011. Distribution of iodide and iodate in the Atlantic sector of the southern ocean during austral summer. *Deep Sea Res. Part II* 58, 2733–2748.
Boscolo-Galazzo, F., Crichton, K.A., Ridgwell, A., Mawbey, E.M., Wade, B.S., Pearson, P. N., 2021. Temperature controls carbon cycling and biological evolution in the ocean twilight zone. *Science* 371, 1148–1152.
Boscolo-Galazzo, F., Jones, A., Dunkley, J.T., Crichton, K.A., Wade, B.S., Pearson, P.N., 2022. Late Neogene evolution of modern deep-dwelling plankton. *Biogeosciences* 19, 743–762.
Boyer, T.P., Baranova, O.K., Coleman, C., Garcia, H.E., Grodsky, A., Locarnini, R.A., Mishonov, A.V., Paver, C.R., Reagan, J.R., Seidov D., Smolyar, I.V., Weathers, K., Zweng, M.M., 2018. World Ocean Database.
Campos, M.L.A.M., Sanders, R., Jickells, T., 1999. The dissolved iodate and iodide distribution in the South Atlantic from the Weddell Sea to Brazil. *Mar. Chem.* 65, 167–175.
Chance, R., Malin, G., Jickells, T., Baker, A.R., 2007. Reduction of iodate to iodide by cold water diatom cultures. *Mar. Chem.* 105, 169–180.
Chance, R., Weston, K., Baker, A.R., Hughes, C., Malin, G., Carpenter, L., Meredith, M.P., Clarke, A., Jickells, T.D., Mann, P., Rossetti, H., 2010. Seasonal and interannual variation of dissolved iodine speciation at a coastal Antarctic site. *Mar. Chem.* 118, 171–181.
Chance, R., Baker, A.R., Carpenter, L., Jickells, T.D., 2014. The distribution of iodide at the sea surface. *Environ. Sci.: Processes Impacts* 16, 1841–1859.
Cheng, K., Ridgwell, A., Hardisty, D., 2024. Characterizing the marine iodine cycle and its relationship to ocean deoxygenation in an Earth System model. *Egusphere* 1–35.
Cléroux, C., Cortijo, E., Anand, P., Labeyrie, L., Bassinot, F., Caillon, N., Duplessy, J.-C., 2008. Mg/Ca and Sr/Ca ratios in planktonic foraminifera: Proxies for upper water column temperature reconstruction: Mg/Ca and Sr/Ca thermometry. Paleoceanography 23, PA3214.
Cobb, K.M., Charles, C.D., Cheng, H., Edwards, R.L., 2003. El Niño/Southern Oscillation and tropical Pacific climate during the last millennium. *Nature* 424, 271–276.
Councell, T.B., Landa, E.R., Lovley, D.R., 1997. Microbial reduction of iodate. *Water Air Soil Pollut.* 100, 99–106.
Cutter, G.A., 2017. Arsenate, iodide, and selenium concentrations collected from Go-FLO bottles during the R/V Thomas G. Thompson Cruise TN303 from Peru to Tahiti in 2013 (U.S. GEOTRACES EPZT Project).
Cutter, G.A., Moffett, J.W., Nielsdóttir, M.C., Sanial, V., 2018. Multiple oxidation state trace elements in suboxic waters off Peru: In situ redox processes and advective/diffusive horizontal transport. *Mar. Chem.* 201, 77–89.
Davis, C.V., Wishner, K., Renema, W., Hull, P.M., 2021. Vertical distribution of planktic foraminifera through an Oxygen Minimum Zone:how assemblages and shell morphology reflect oxygen concentrations. Paleobiogeoscience: Marine Record.
Duplessy, J.C., Bé, A.W.H., Blanc, P.L., 1981. Oxygen and carbon isotopic composition and biogeographic distribution of planktonic foraminifera in the Indian Ocean. *Palaeogeogr. Palaeoclimatol. Palaeoecol.* 33, 9–46.
Elderfield, H., Truesdale, V.W., 1980. On the biophilic nature of iodine in seawater. *Earth Planet. Sci. Lett.* 50, 105–114.
Engel, A., Kiko, R., Dengler, M., 2022. Organic matter supply and utilization in oxygen minimum zones. *Annu. Rev. Mar. Sci.* 14, 355–378.
Evans, N., Johnson, E., Taing, A., Schnur, A.A., Chace, P.J., Richards, S., Hardisty, D.S., Moffett, J.W., 2024. More Than Deoxygenation: Linking Iodate Reduction to Nitrogen, Iron, and Sulfur Chemistry in Reducing Regimes. J. Geophys. Res.: Oceans 129, e2024JC021013.
Farrenkopf, A.M., Luther, G.W., 2002. Iodine chemistry reflects productivity and denitrification in the Arabian Sea: evidence for flux of dissolved species from sediments of western India into the OMZ. *Deep Sea Res. Part II* 49, 2303–2318.

Farrenkopf, A.M., Luther, G.W., Truesdale, V.W., Van Der Weijden, C.H., 1997. Subsurface iodide maxima: evidence for biologically catalyzed redox cycling in Arabian Sea OMZ during the SW intermonsoon. *Deep Sea Res. Part II* 44, 1391–1409.

Faul, K.L., Ravelo, C.A., Delaney, M.L., 2000. Reconstructions of upwelling, productivity, and photic zone depth in the eastern equatorial Pacific Ocean using planktonic foraminiferal stable isotopes and abundances. *J. Foraminiferal Res.* 30, 110–125.

Fehrenbacher, J.S., Russell, A.D., Davis, C.V., Spero, H.J., Chu, E., Hönisch, B., 2018. Ba/Ca ratios in the non-spinose planktic foraminifer *Neogloboquadrina dutertrei*: Evidence for an organic aggregate microhabitat. *Geochim. Cosmochim. Acta* 236, 361–372.

Fiedler, P.C., Talley, L.D., 2006. Hydrography of the eastern tropical Pacific: a review. *Prog. Oceanogr.* 69, 143–180.

Fuenzalida, R., Schneider, W., Garcés-Vargas, J., Bravo, L., Lange, C., 2009. Vertical and horizontal extension of the oxygen minimum zone in the eastern South Pacific Ocean. *Deep Sea Res. Part II* 56, 992–1003.

German, C.R., 2017. Core-top (0-1cm) sediment data collected by monocore from R/V Thomas G. Thompson TN303 (GP16; EPZT). GEOTRACES Cruise from November to December 2013 (GEOTRACES EPZT Project).

Glock, N., Liebetrau, V., Eisenhauer, A., 2014. I/Ca ratios in benthic foraminifera from the Peruvian oxygen minimum zone: analytical methodology and evaluation as a proxy for redox conditions. *Biogeosciences* 11, 7077–7095.

Glock, N., Liebetrau, V., Eisenhauer, A., Rocholl, A., 2016. High resolution I/Ca ratios of benthic foraminifera from the Peruvian oxygen-minimum-zone: A SIMS derived assessment of a potential redox proxy. *Chem. Geol.* 447, 40–53.

Hardisty, D.S., Lu, Z., Planavsky, N.J., Bekker, A., Philippot, P., Zhou, X., Lyons, T.W., 2014. An iodine record of Paleoproterozoic surface ocean oxygenation. *Geology* 42, 619–622.

Hardisty, D.S., Lu, Z., Bekker, A., Diamond, C.W., Gill, B.C., Jiang, G., Kah, L.C., Knoll, A. H., Loyd, S.J., Osburn, M.R., Planavsky, N.J., Wang, C., Zhou, X., Lyons, T.W., 2017. Perspectives on Proterozoic surface ocean redox from iodine contents in ancient and recent carbonate. *Earth Planet. Sci. Lett.* 463, 159–170.

Hardisty, D.S., Horner, T.J., Evans, N., Moriyasu, R., Babbin, A.R., Wankel, S.D., Moffett, J.W., Nielsen, S.G., 2021. Limited iodate reduction in shipboard seawater incubations from the Eastern Tropical North Pacific oxygen deficient zone. *Earth Planet. Sci. Lett.* 554, 116676.

Helly, J.J., Levin, L.A., 2004. Global distribution of naturally occurring marine hypoxia on continental margins. *Deep Sea Res. Part I* 51, 1159–1168.

Hepach, H., Hughes, C., Hogg, K., Collings, S., Chance, R., 2020. Senescence as the main driver of iodide release from a diverse range of marine phytoplankton. *Biogeosciences* 17, 2453–2471.

Hess, A.V., Auderset, A., Rosenthal, Y., Miller, K.G., Zhou, X., Sigman, D.M., Martínez-García, A., 2023. A well-oxygenated eastern tropical Pacific during the warm Miocene. *Nature* 619, 521–525.

Hollstein, M., Mohtadi, M., Rosenthal, Y., Moffa, S.P., Oppo, D., Martínez, M.G., Steinke, S., Hebbeln, D., 2017. Stable Oxygen Isotopes and Mg/Ca in Planktic Foraminifera From Modern Surface Sediments of the Western Pacific Warm Pool: Implications for Thermocline Reconstructions. *Paleoceanography* 32, 1174–1194.

Hoogakker, B.A.A., Lu, Z., Umling, N., Jones, L., Zhou, X., Rickaby, R.E.M., Thunell, R., Cartapanis, O., Galbraith, E., 2018. Glacial expansion of oxygen-depleted seawater in the eastern tropical Pacific. *Nature* 562, 410–413.

Hutson, W.H., 1977. Variations in planktonic foraminiferal assemblages along north–south transects in the Indian Ocean. *Mar. Micropaleontol.* 2, 47–66.

Jiang, S., Zhou, X., Sachs, J.P., Li, Z., Tu, L., Lin, Y., Liu, X., Chen, A., Shen, Y., 2023. The mean state of the tropical Pacific Ocean differed between the Medieval Warm Period and the Industrial Era. *Commun. Earth Environ.* 4, 1–9.

Jickells, T.D., Boyd, S.S., Knap, A.H., 1988. Iodine cycling in the Sargasso Sea and the Bermuda inshore waters. *Mar. Chem.* 24, 61–82.

Jonkers, L., De Nooijer, L.J., Reichart, G.-J., Zahn, R., Brummer, G.-J.-A., 2012. Encrustation and trace element composition of *Neogloboquadrina dutertrei* assessed from single chamber analyses – implications for paleotemperature estimates. Biogeosciences 9, 4851–4860.

Kalansky, J., 2014. Internal and forced variability of the equatorial Pacific on millenial and centennial time scales. The State University of New Jersey, Rutgers.

Karstensen, J., Stramma, L., Visbeck, M., 2008. Oxygen minimum zones in the eastern tropical Atlantic and Pacific oceans. *Prog. Oceanogr.* 77, 331–350.

Kessler, W.S., 2006. The circulation of the eastern tropical Pacific: A review. *Prog. Oceanogr.* 69, 181–217.

Kim, R.A., Lee, K.E., Ko, T.W., 2023. Seasonal and vertical distribution of living planktonic foraminifera in the western tropical Pacific Ocean. *Deep Sea Res. Part I* 201, 104159.

Lu, Z., Jenkyns, H.C., Rickaby, R.E.M., 2010. Iodine to calcium ratios in marine carbonate as a paleo-redox proxy during oceanic anoxic events. *Geology* 38, 1107–1110.

Lu, Z., Hoogakker, B.A.A., Hillenbrand, C.-D., Zhou, X., Thomas, E., Gutchess, K.M., Lu, W., Jones, L., Rickaby, R.E.M., 2016. Oxygen depletion recorded in upper waters of the glacial Southern Ocean. *Nat Commun* 7, 11146.

Lu, W., Wörndle, S., Halverson, G.P., Zhou, X., Bekker, A., Rainbird, R.H., Hardisty, D.S., Lyons, T.W., Lu, Z., 2017. Iodine proxy evidence for increased ocean oxygenation during the Bitter Springs Anomaly. *Geochem. Persp. Let.* 53–57.

Lu, W., Ridgwell, A., Thomas, E., Hardisty, D.S., Luo, G., Algeo, T.J., Saltzman, M.R., Gill, B.C., Shen, Y., Ling, H.-F., Edwards, C.T., Whalen, M.T., Zhou, X., Gutchess, K. M., Jin, L., Rickaby, R.E.M., Jenkyns, H.C., Lyons, T.W., Lenton, T.M., Kump, L.R., Lu, Z., 2018. Late inception of a resiliently oxygenated upper ocean. *Science*.

Lu, W., Dickson, A.J., Thomas, E., Rickaby, R.E.M., Chapman, P., Lu, Z., 2020a. Refining the planktic foraminiferal I/Ca proxy: Results from the Southeast Atlantic Ocean. *Geochim. Cosmochim. Acta* 287, 318–327.

Lu, W., Rickaby, R.E.M., Hoogakker, B.A.A., Rathburn, A.E., Burkett, A.M., Dickson, A.J., Martínez-Méndez, G., Hillenbrand, C.-D., Zhou, X., Thomas, E., Lu, Z., 2020b. I/Ca in epifaunal benthic foraminifera: a semi-quantitative proxy for bottom water oxygen in a multi-proxy compilation for glacial ocean deoxygenation. *Earth Planet. Sci. Lett.* 533, 116055.

Lu, W., Barbosa, C.F., Rathburn, A.E., Xavier, P. da M., Cruz, A.P.S., Thomas, E., Rickaby, R.E.M., Zhang, Y.G., Lu, Z., 2021. Proxies for paleo-oxygenation: A downcore comparison between benthic foraminiferal surface porosity and I/Ca. *Palaeogeogr. Palaeoclimatol. Palaeoecol.* 579, 110588.

Lu, Z., Thomas, E., Rickaby, R., Lu, W., Prow, A., 2023. Commentary: Planktic foraminifera iodine/calcium ratios from plankton tows. Front. Marine Sci. 10.

Lu, W., Wang, Y., Oppo, D.W., Nielsen, S.G., Costa, K.M., 2022. Comparing paleo-oxygenation proxies (benthic foraminiferal surface porosity, I/Ca, authigenic uranium) on modern sediments and the glacial Arabian Sea. *Geochim. Cosmochim. Acta* 331, 69–85.

Luther, G.W.I., 2023. Review on the physical chemistry of iodine transformations in the oceans. *Front. Mar. Sci.* 10.

Mann, M.E., Zhang, Z., Rutherford, S., Bradley, R.S., Hughes, M.K., Shindell, D., Ammann, C., Faluvegi, G., Ni, F., 2009. Global signatures and dynamical origins of the little ice age and medieval climate anomaly. *Science* 326, 1256–1260.

Margolskee, A., Frenzel, H., Emerson, S., Deutsch, C., 2019. Ventilation pathways for the North Pacific oxygen deficient zone. *Global Biogeochem. Cycles* 33, 875–890.

Moffett, J., Cutter, G., German, C., 2020. GTC CTD down casts along the US GEOTRACES East Pacific Zonal Transect from the R/V Thomas G. Thompson TN303 Cruise in the Tropical Pacific from Peru to Tahiti during 2013 (U.S. GEOTRACES EPZT Project).

Moriyasu, R., Evans, N., Bolster, K.M., Hardisty, D.S., Moffett, J.W., 2020. The distribution and redox speciation of iodine in the eastern tropical North Pacific Ocean. *Global Biogeochem. Cycles* 34.

Moriyasu, R., Bolster, K.M., Hardisty, D.S., Kadko, D.C., Stephens, M.P., Moffett, J.W., 2023. Meridional Survey of the Central Pacific Reveals Iodide Accumulation in Equatorial Surface Waters and Benthic Sources in the Abyssal Plain. *Global Biogeochem. Cycles* 37.

Regenberg, M., Nürnberg, D., Steph, S., Groeneveld, J., Garbe-Schönberg, D., Tiedemann, R., Dullo, W.-C., 2006. Assessing the effect of dissolution on planktonic foraminiferal Mg/Ca ratios: Evidence from Caribbean core tops. *Geochemistry Geophysics, Geosystems* 7.

Rosenthal, Y., Field, M.P., Sherrell, R.M., 1999. Precise determination of element/calcium ratios in calcareous samples using sector field inductively coupled plasma mass spectrometry. *Anal. Chem.* 71, 3248–3253.

Rue, E.L., Smith, G.J., Cutter, G.A., Bruland, K.W., 1997. The response of trace element redox couples to suboxic conditions in the water column. *Deep Sea Res. Part I* 44, 113–134.

Rustic, G.T., Koutavas, A., Marchitto, T.M., Linsley, B.K., 2015. Dynamical excitation of the tropical Pacific Ocean and ENSO variability by Little Ice Age cooling. *Science* 350, 1537–1541.

Schott, F.A., Mccreary, Jr. J.P., Johnson, G.C., 2004. Shallow Overturning Circulations of the Tropical-Subtropical Oceans. In: Earth's Climate American Geophysical Union (AGU). pp. 261–304.

Stramma, L., Schmidtko, S., 2021. Tropical deoxygenation sites revisited to investigate oxygen and nutrient trends. Ocean Sci. 17 (3), 833–847.

Taylor, M.A., Hendy, I.L., Chappaz, A., 2017. Assessing oxygen depletion in the Northeastern Pacific Ocean during the last deglaciation using I/Ca ratios from multiple benthic foraminiferal species. *Paleoceanography* 32, 746–762.

Tsunogai, S., Henmi, T., 1971. Iodine in the surface water of the ocean. *J. Oceanogr. Soc. Jpn.* 27, 67–72.

Wadley, M.R., Stevens, D.P., Jickells, T.D., Hughes, C., Chance, R., Hepach, H., Tinel, L., Carpenter, L.J., 2020. A global model for iodine speciation in the upper ocean. *Global Biogeochem. Cycles* 34, e2019GB006467.

Watkins, J.M., Mix, A.C., Wilson, J., 1996. Living planktic foraminifera: tracers of circulation and productivity regimes in the central equatorial Pacific. *Deep Sea Res. Part II* 43, 1257–1282.

Winkelbauer, H.A., Hoogakker, B.A.A., Chance, R.J., Davis, C.V., Anthony, C.J., Bischoff, J., Carpenter, L.J., Chenery, S.R.N., Hamilton, E.M., Holdship, P., Peck, V. L., Poulton, A.J., Stinchcombe, M.C., Wishner, K.F., 2023. Planktic foraminifera iodine/calcium ratios from plankton tows. *Front. Marine Sci.* 10.

Wong, G.T.F., 1991. The marine geochemistry of iodine. *Rev. Aquat. Sci.* 4, 45–73.

Wong, G.T.F., Brewer, P.G., 1977. The marine chemistry of iodine in anoxic basins. *Geochim. Cosmochim. Acta* 41, 151–159.

Ying, R., Monteiro, F.M., Wilson, J.D., Schmidt, D.N., 2023. ForamEcoGEnIE 2.0: incorporating symbiosis and spine traits into a trait-based global planktic foraminiferal model. *Geosci. Model Dev.* 16, 813–832.

Zhang, J., Liang, M.-Q., Li, T.-Y., Chen, C.-J., Li, J.-Y., 2022. Asian-Australian monsoon evolution over the last millennium linked to ENSO in composite stalagmite $\delta^{18}O$ records. Quat. Sci. Rev. 281, 107420.

Zhou, X., Thomas, E., Rickaby, R.E.M., Winguth, A.M.E., Lu, Z., 2014. I/Ca evidence for upper ocean deoxygenation during the PETM. *Paleoceanography* 29, 964–975.

Zhou, X., Jenkyns, H.C., Owens, J.D., Junium, C.K., Zheng, X.-Y., Sageman, B.B., Hardisty, D.S., Lyons, T.W., Ridgwell, A., Lu, Z., 2015. Upper ocean oxygenation dynamics from I/Ca ratios during the Cenomanian-Turonian OAE 2: I/Ca and ocean oxygenation across OAE2. Paleoceanography 30, 510–526.

Zhou, X., Hess, A.V., Bu, K., Sagawa, T., Rosenthal, Y., 2022. Simultaneous determination of I/Ca and other elemental ratios in foraminifera using sector field ICP-MS. *Geochem. Geophys. Geosyst.* 23, e2022GC010660.